On the Performance of Point Kinetics for the Analysis of Accelerator Driven Systems

M. Eriksson*

Royal Institute of Technology, Stockholm Center for Physics, Astronomy and Biotechnology, Dep. Nuclear & Reactor Physics, 10691 Stockholm, Sweden.

and

J. E. Cahalan and W. S. Yang

Argonne National Laboratory, Nuclear Engineering Division, 9700 South Cass Ave., IL 60439, USA.

Abstract – *The ability of point kinetics to describe dynamic processes in accelerator-driven systems (ADS) is investigated. Full three-dimensional energy-space-time dependent calculations, coupled with thermal- and hydraulic feedback effects, are performed and used as a standard of comparison. Various transient accident sequences are studied. Calculations are performed in the range of k_{eff} = 0.9594 to 0.9987, to provide insight into the dependence of the performance on the subcritical level. Numerical experiments are carried out on a minor-actinide loaded and lead-bismuth cooled ADS. It is shown that the point kinetics approximation is capable of providing highly accurate calculations in such systems. The results suggest better precision at lower k_{eff}-levels. It is found that subcritical operation provides features that are favorable from a point kinetics view of application. For example, reduced sensitivity to system reactivity perturbations effectively mitigates any spatial distortions. If a subcritical reactor is subject to a change in the strength of the external source, or a change in reactivity within the subcritical range, the neutron population will adjust to a new stationary level. Therefore, within the normal range of operation, the power predicted by the point kinetics method and the associated error in comparison with the exact solution tends to approach an essentially bounded value. It was found that the point kinetics model is likely to underestimate the power rise following a reactivity insertion in an ADS, which is similar to the behavior in critical systems.*

I. INTRODUCTION

In recent years, there has been an increasing interest in the application of accelerator-driven systems (ADS) for the purpose of incinerating long-lived radionuclides in high-level waste. The ADS is a non-self-sustaining, subcritical reactor driven by an external neutron source that is maintained by a charged-particle accelerator. Appropriate neutron kinetics models are required for predicting the consequences of operational disturbances and accidents in these systems. The so-called "point kinetics approximation" is a widely used method for performing preliminary analyses of dynamic phenomena. It has been extensively applied for the transient design analysis of existing reactors and it forms the basis of many transient analysis computational codes. It is based on kinetics theory developed for critical reactor studies. While the utility of the point kinetics methodology for critical reactor analysis is well known, its applicability to source-driven subcritical systems is subject to investigation[1]. Because the neutron balance equations that describe the response in source-driven reactors are fundamentally different from the problem characterizing critical reactors, it has been suggested[2] that the point kinetics technique may be inappropriate for ADS studies; it is nonetheless very popular and often used for analysing such systems.

In the present paper, we investigate the precision of the point model in its application to ADS in some more detail. The objective is to estimate the magnitude of the errors encountered in the analysis of certain accidents under physically realistic conditions, i.e., including thermal- and hydraulic feedbacks. The basic approach is by comparison with an "exact" numerical solution. Results are obtained as function of the subcritical level. First, we make a short review of point kinetics theory and discuss its implications in a source-driven, subcritical operating mode. We then describe the test models and the computational techniques involved in the study. Problems and results are then summarized, followed by a brief conclusion in the last section.

*E-mail: marcus@neutron.kth.se

II. REACTOR KINETICS EQUATIONS

In this section, we review shortly the derivation of the conventional kinetics equations. These were first derived by Henry[3]. Their limitations and capabilities for critical reactor analysis have been investigated in great detail[4-6]. The derivation is presented here to serve as a basis for discussion of applications to source-driven systems. For convenience, the derivation proceeds along the lines suggested by Henry[7] with minor modification. An independent source term is incorporated to include neutrons supplied by the external source. The starting-point is the time-dependent continuous energy diffusion equation[a]. In shorthand operator notation it can be written as:

$$\frac{1}{v}\frac{\partial \Phi}{\partial t} = (\mathbf{F}_p - \mathbf{M})\Phi + \sum_k \lambda_k C_k \chi_{dk} + S \qquad (1a)$$

and completed with the balance equation for the delayed-neutron precursors

$$\frac{\partial C_k}{\partial t} = -\lambda_k C_k + \int_0^\infty \nu_{dk}\Sigma_f(\mathbf{r},E',t)\phi(\mathbf{r},E',t)\,dE' \qquad (1b)$$

$\Phi = \phi(\mathbf{r},E,t)$ is the time-dependent neutron flux. For simplicity of notation, the functional dependence in Eq (1a) and (1b) has been suppressed. **M** and $\mathbf{F_p}$ are the usual "migration and loss operator" and the "prompt neutron production operator", respectively. These correspond to:

$$\mathbf{F}_p\Phi = \chi_p(E)\int_0^\infty \nu_p\Sigma_f(\mathbf{r},E',t)\phi(\mathbf{r},E',t)\,dE'$$

$$\mathbf{M}\Phi = -\nabla\cdot D(\mathbf{r},E,t)\nabla\phi(\mathbf{r},E,t) + \Sigma_t(\mathbf{r},E,t)\phi(\mathbf{r},E,t) - \int_0^\infty \Sigma_s(\mathbf{r},E'\to E,t)\phi(\mathbf{r},E',t)\,dE'$$

The purpose behind the formulation of the kinetics equations is to derive a lumped model that describes the change in the average level of the flux, i.e., the integral of $\phi(\mathbf{r},E,t)$ over the energy and the spatial domain. For that reason, the neutron flux is factorized in the form $\phi(\mathbf{r},E,t) = p(t)\cdot\psi(\mathbf{r},E,t)$. It is noted that flux factorization is not an approximation, in contrast to separation of variables. In the former case, the neutron spatial and energy distributions may still depend on time. However, it is necessary to impose a constraint condition to define precisely the two new functions, *p(t)* and *ψ(**r**,E,t),* that arise in the factorization procedure:

$$\int_V\int_0^\infty \frac{w(\mathbf{r},E)\psi(\mathbf{r},E,t)}{v(E)}\,dEdV = 1 \qquad (2)$$

The constraint condition states that the shape function, *ψ(**r**,E,t),* is normalized, for all t, in such a manner that the integral, Eq. (2), over all energy and space is held constant (normally taken as unity) in time. Prior to integration over space and energy, Eq. (1a) and (1b) is multiplied with a weight function, *w(**r**,E)*. Introducing a weight function is not a requirement, but it allows manipulation of the kinetics equations in a way that simplifying assumptions (such as the point kinetics approximation) can be applied more effectively. It is emphasized, that the weight function can be any function that is defined over the same energy and spatial domain as the flux. To preserve generality, the following derivation will not employ a specific weight function.

p(t) is sometimes called the amplitude function and it is defined according to:

$$p(t) = \int_V\int_0^\infty \frac{w(\mathbf{r},E)\phi(\mathbf{r},E,t)}{v(E)}\,dEdV \qquad (3)$$

Thus, under the constraint condition given in Eq. (2), *p(t)* can be represented as in Eq. (3) and hence it is proportional to the total number of neutrons present in the reactor at any time.

Next, Eq. (1a) and (1b) are multiplied with the weight function and the neutron flux is substituted with the factorized functions. The equations are then integrated with respect to space and energy. After some manipulations, we arrive at the conventional point kinetics equations:

$$\frac{dp(t)}{dt} = \frac{\rho(t)-\beta(t)}{\Lambda(t)}p(t) + \sum_k \lambda_k c_k(t) + s(t) \qquad (4a)$$

$$\frac{dc_k(t)}{dt} = \frac{\beta_k(t)}{\Lambda(t)}p(t) - \lambda_k c_k(t) \qquad (4b)$$

The new quantities, ρ, β, Λ, s, and c_k that emerge in Eqs. (4) are the integral quantities identified with the following definitions:

$$\beta(t) = \sum_k \beta_k(t)$$

$$\beta_k(t) = \frac{1}{F(t)}\int\int w\sum_k \mathbf{F}_{dk}\psi\,dEdV$$

$$\rho(t) = \frac{\int\int w(\mathbf{F}_p - \mathbf{M})\psi\,dEdV}{F(t)}$$

$$\Lambda(t) = \frac{1}{F(t)}\int\int \frac{w\psi}{v}\,dEdV$$

$$s(t) = \frac{\int\int wS\,dEdV}{\int\int \frac{w\psi}{v}\,dEdV}$$

$$c_k(t) = \frac{\int\int wC_k\chi_{dk}\,dEdV}{\int\int \frac{w\psi}{v}\,dEdV}$$

[a] In his original work[3], Henry derived the reactor kinetics equations starting from the time dependent neutron transport equation, we chose not to proceed along this path, but rather to utilize the diffusion approach as outlined in his textbook[7], mainly to be in better accordance with the terms of our computational exercises and to avoid the potential of being misleading. In general, the reactor kinetics equations involve angular dependence and as shown by Henry, the equations may be extended to a transport formulation in a straightforward manner.

The definition of F(t) is:

$$F(t) = \int\int w(\mathbf{F}_p + \sum_k \mathbf{F}_{dk})\psi \, dEdV$$

where the delayed neutron production operators $\mathbf{F}_{dk}$ are defined similar to the prompt neutron production operator. It is in the cross sections (that depend on temperature, material density, and composition) in the operators $\mathbf{F}_p$ and $\mathbf{M}$ that thermal and hydraulic feedbacks are accounted for during a transient.

Henry[3], called Eqs. (4) the "conventional kinetics equations". Today they are usually referred to as the "point kinetics equations" or sometimes the "exact point kinetics equations" in a way to distinguish them from the simplifying assumptions applied in the point kinetics approximation.

It is stressed that Eqs. (4) are exact and completely equivalent to Eqs. (1), but in a different form. The basic, time-dependent equations, Eqs. (1), are recast into Eqs. (4) without simplifying approximations. Henry[7] clearly states that as long as the rigorous definitions of the kinetics parameters are used, i.e., the actual time-dependent flux shape is calculated, the solution of Eqs. (4) for *p(t)* with any arbitrary weighting function will be *exactly* the same as the solution of Eqs. (1) for $\phi(\mathbf{r},E,t)$ and then the application of Eq. (3). This is true for critical as well as for subcritical systems. The error is introduced when we modify the equations to better cope with an approximate representation of the time-dependent flux shape, e.g., the point kinetics approximation. In that case, the weight function becomes useful because it leaves us with the possibility of freely choosing $w(\mathbf{r},E)$ in a manner to better suit a point kinetics approximation. Within a perturbation theory approach it is shown[7] for a critical reactor, that adjoint flux weighting eliminates the influence of first-order flux shape changes on the reactivity, and therefore also reduces the error in the approximation of *p(t)*. Consequently, the estimation for *p(t)* may tolerate a less precise description of the flux shape. This fact facilitates the use of the initial flux shape throughout the entire transient, i.e., first-order perturbation theory approach. In first-order perturbation theory, the weight function corresponds to the initial adjoint flux, $\Phi^*_{\lambda_0}$, i.e., the solution of the initial adjoint eigenvalue problem:

$$(\mathbf{M}_0^* - \lambda_0 \mathbf{F}_0^*)\Phi^*_{\lambda_0} = 0 \qquad (5)$$

Where $\mathbf{F}_0^*$ and $\mathbf{M}_0^*$ are the adjoint operators of the total neutron production operator, $\mathbf{F}_0 = \mathbf{F}_{p0} + \sum_k \mathbf{F}_{dk0}$, and the loss operator $\mathbf{M}_0$. In the point kinetics approximation, the basic assumption is that the time dependence is separable from the $(\mathbf{r},E)$ dependence, i.e, the space-energy flux shape is fixed at all times. For a critical reactor, it permits the use of first-order perturbation theory to calculate the reactivity changes. The neutron balance equation for a reactor with an independent source is mathematically an inhomogeneous problem. In strict terms, separation of variables is not possible for such cases. Thus, the point kinetics approximation becomes questionable. Moreover, the adjoint flux is not uniquely defined for a source-driven system. This invalidates the use of the standard first-order perturbation formula. The usual procedure for generating a weight function for a source-driven reactor is to employ an artificial initial λ-mode adjoint weighting function, i.e., the solution to the source-free adjoint equation, Eq. (5). As was shown by Ott[8], the error cancellation property of the first-order perturbation formula is preserved in a source-driven system if the real flux shape is calculated from the initial inhomogeneous problem and not the initial λ-mode shape.

The integral kinetics parameters ρ, β, and Λ arise only in the derivation of lumped models such as the kinetics equations. This is realized since Eqs. (1) do not involve these concepts. It is noted that the point kinetics parameters depend on the weighting function and for that reason their definition is entirely arbitrary. Therefore, the kinetics parameters do not necessarily correspond to any physically meaningful quantities. According to Henry[3], the kinetics parameters have a meaningful interpretation only when the reactor is on a constant reactivity level and when the independent source term is negligible in comparison with the fission rate. These conditions are fulfilled automatically in a critical reactor when the time dependence is separable from the $(\mathbf{r},E)$ dependence. If the weighting function is unity then a clear physical interpretation can be defined. If $w(\mathbf{r},E)\neq 1$ then the kinetics parameters correspond to some weighted physical value. Using the adjoint flux as weighting function, $w(\mathbf{r},E)=\phi(\mathbf{r},E)^*$, has the benefit of producing "importance" weighted kinetics parameters. These can sometimes be interpreted as "effective" values. Since a source-free adjoint weighting function does not correspond to the actual state of a source-driven system the physical meaning of the point kinetics parameters is not clear. However, according to Becker[9], a complication also arises in a critical system because the weighting function employed in the point kinetics equations is time-independent, nevertheless the adjoint function might change during a transient. In that case, it might not correspond to the actual physical state.

III. TEST MODEL

The model used in the present study is based on a previous OECD/NEA benchmark model[10] with some minor modifications[b,c]. The original benchmark was not intended as a transient case study, but adopting this system as the basis for the current tests has the benefit that initial static results could be compared with previous studies.

[b]The r-z geometry specification prescribed in the benchmark was converted to a three-dimensional hexagonal-z representation.

[c]To avoid computational artefacts due to the treatment of void regions with a diffusion theory approach, the current model assumes that the coolant fills the full extent of the target and the beam duct region.

The model pertains to an accelerator-driven, lead-bismuth cooled, and minor-actinide loaded transmuter core. The core consists of a central lead-bismuth target region and a homogenized fuel region surrounded by radial and axial reflectors (70% steel and 30% coolant). 114 fuel assemblies are included in the hexagonal-z representation; Fig 1 contains a plan view of a one-sixth symmetry section of the core. The height of the active core is 100 cm. The fuel consists of 2/3 minor actinides and 1/3 plutonium with a ZrN diluent; $(Pu_{0.1},MA_{0.2},Zr_{0.7})N$, where MA represents minor actinides such as Np, Am, and Cm. Fuel compositions correspond to plutonium discharge from UOX-fueled LWRs mixed with MA from a "double strata" strategy[11]. Start-up core loading is used in the simulations. The fuel is further diluted with 71% ZrN. Core material compositions are summarized in TABLE I. Additional lattice parameters are included in TABLE II.

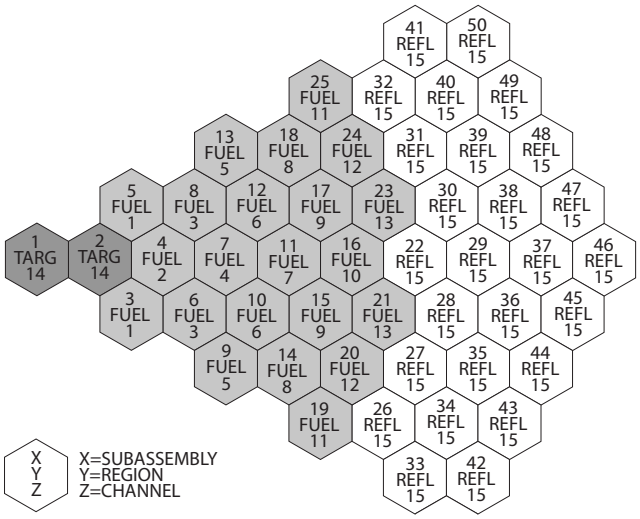

Fig 1. One-Sixth Core Subassembly and Channel Assignment.

TABLE I
Material Specification of the Reference Core Configuration

Core Volume Fractions:
30 vol% Fuel
48 vol% Coolant (Pb/Bi eutectic)
22 vol% Clad + Structure (stainless steel)
Reflector Volume Fractions:
30 vol% Coolant
70 vol% Stainless Steel
Fuel:
Fuel Material: $(Pu_{0.1},MA_{0.2},Zr_{0.7})N$
Theoretical density (300°C): 9.19 g/cm^3
Fuel smear density: 84 % of theoretical
68% MA/TRU ratio
71% molar fraction ZrN

TABLE II
Lattice parameters

Number of pins per assembly	217
Pitch/diameter ratio	1.6
Pin diameter [mm]	7.366
Cladding thickness [mm]	0.787
Ducts flat-to-flat distance [cm]	15.956

IV. COMPUTATIONAL MODELING TECHNIQUES

Numerical testing was performed with coupled core dynamics calculations using the SAS4A/DIF3D-K[12] code. The "exact" results are obtained from a direct numerical solution of the time-, space-, and energy-dependent multigroup diffusion equation. The direct solution is used as a standard of comparison for the point kinetics solution. One advantage of using the SAS4A/DIF3D-K program for the current task is that the direct solution method and the point kinetics procedure are implemented within the same code. This makes it straightforward to compare the underlying methods without worrying about consistency among different computational procedures and models. For example, the initial steady-state solutions, cross sections, thermal- and hydraulics treatments, and model specifications are all identical.

Thirty-three energy groups are employed in the multi-group treatment. Composition-, temperature- and region-dependent broad group microscopic cross sections were generated based on JEF2.2 data and further processed using the MC^2-2[13] and TWODANT[14] codes. With MC^2-2, a homogeneous, ultra-fine group (2082 groups), zero-dimensional spectrum calculation (infinite medium assumption) is first performed for each composition. Individual material microscopic cross sections are reduced to the fine group level (230 groups) by averaging the ultra-fine-group data over the flux and current spectra. Full-core fine group calculations are then carried out with TWODANT. The spectra obtained from TWODANT are used to spatially collapse the fine-group data to a broad group level (33 groups). The broad-group microscopic cross sections are composition-, region- and temperature dependent, i.e., different sets of cross sections for different regions and temperatures (500 K, 980 K, 1580 K, and 2500 K). Local cross sections used in the transient flux calculations are obtained through interpolation in these sets to fit a particular temperature.

Data for delayed neutrons and their precursors were generated based on the ENDF/B-VI library. Delayed neutron data for fissioned curium isotopes was not available in ENDF/B-VI. The missing curium isotopes adopted the delayed neutron yield of ^{239}Pu.

An external neutron source distribution was supplied in the specification of the benchmark[10]. The neutrons are produced by spallation nuclear reactions induced by high-energy protons impinging on a lead-bismuth target. The target has a height of 100 cm and a radius of 20 cm. The

energy of the incident protons is 1 GeV and the beam has a radius of 10 cm. The fine group source (122 groups) is collapsed to a broad group level (33 groups) and the r-z representation was converted to hexagonal-z geometry. The source neutrons are presumed to enter the system at the target meshes. The temporal dependence of the external source intensity enters the SAS4A/DIF3D-K code as one of the system driving functions. For transients involving alterations of the source strength, it is assumed that the neutron spatial and energy distributions are maintained during the transients; i.e., only the magnitude of the external neutron source is adjusted. This is a reasonable assumption since the spatial and energy distributions of the source neutrons depend on the proton beam energy and the target and core configuration, which are fixed during the transients.

The spatial flux solutions are based on a three-dimensional nodal diffusion theory method[15]. The core is partitioned into assembly-sized hexagonal unit cells in the horizontal planar direction and axially subdivided into twenty-one axial nodes, each with a mesh spacing of 4.76 cm. In reflector regions, axial mesh sizes of 12.5 cm are employed. The radial distance between the assembly vertical centerlines is 16 cm. The solution takes advantage of one-sixth core symmetry by solving for a single sextant section of the core. Uniform nuclear cross sections are used within each node. In the direct method, the time-dependent component is solved using a fully implicit finite-difference approximation (the DIF3D-K[16] code uses a specified θ-method[17] of time differencing). The theta (θ=1) method consists of representing the time differential operators with their implicit finite-difference formulation. Thermal- and hydraulic calculations are performed for 13 channels, each representative of an average pin within individual subassemblies (See Fig 1 for channel to subassembly assignments). Feedback effects (due to Doppler and coolant density variations) are included as necessary to reproduce the physical situation as closely as possible. Both the direct solution and the point kinetics method account for thermal feedbacks through node-dependent microscopic and macroscopic cross sections. The cross sections are updated with time as local temperatures and densities changes. In the point kinetics solution, the initial flux shape is used throughout the entire transient calculation. Time-dependent point kinetics parameters are computed by means of first-order perturbation theory. The initial flux shape, determined with a given external source distribution, and the initial λ-mode adjoint flux are used along with macroscopic cross sections to compute time-dependent point kinetics parameters, especially the reactivity parameter which reflects the thermal feedbacks. The reactivity is found by summing contributions from local changes in temperature and material densities (as opposed to the use of core-average reactivity coefficients). The adjoint flux is required in the evaluation of the scalar products used in the calculation of the time-dependent kinetics parameters. It corresponds to the initial source-free mathematical nodal adjoint solution[18]. The direct solution technique does not require the formulation of kinetics parameters and adjoint fluxes. The great advantage of the direct solution is that an unambiguous and "exact" solution of the inhomogeneous time-dependent group diffusion equation is obtained, in that sense that no approximations is introduced other than space nodalization and time differencing.

Transient solutions are obtained using a fixed time step size[d] of Δt=10 ms (results for test problems employing smaller time steps suggested that a time increment of 10 ms is adequate for the current set of problems). At the end of each time step, new cross sections are calculated. Heat-transfer and hydraulics time-steps are on separate sub-steps.

V. NUMERICAL RESULTS

Numerical solutions for three different categories of transients were analyzed. The test problems pertain to accident-type events in ADS's. The first category concerns alterations of the proton beam intensity, i.e., changes in the magnitude of the external neutron source. Secondly, localized reactivity insertions are examined. Finally, a flow reduction event is analyzed. The total power is extracted as a function of time, i.e., fission power plus decay power, as obtained in the direct solution and in the point kinetics solution. The transients are followed for 20.0 seconds.

We further perform calculations at different subcritical levels, i.e., k_{eff} values, to reveal any trends concerning performance characteristics. It will provide information on the numerical accuracy of the point kinetics solution as function of the level of subcriticality. The multiplication constant is altered by changing the concentration of fuel diluents (ZrN), everything else is unchanged, initial k_{eff} values are given in TABLE III. Unless the source strength is adjusted, an increase in k_{eff} would lead to a higher power output. Thus, the intensity of the external source is adjusted to maintain the initial power at 377 MWth. Results from the calculation of the initial effective multiplication constant, shown in TABLE III, proved to be in good agreement with previous results[10].

TABLE III
Initial effective multiplication constant (hot condition)

Case	Fraction ZrN	k_{eff}
Case 1 (ref.)	70.7%	0.9594
Case 2	69.4%	0.9798
Case 3	68.2%	0.9987

[d]It ought to be clarified that the time-dependent flux solution in DIF3D-K employs an automatic time-step selection algorithm[19], which monitors the rate of change of the fission source and constrains the time-step based on a user-specified value. However, the specified time step was sufficiently small that it prevailed in all test cases.

V.A. Variations in Source Strength

In an ADS, the traditional reactivity based shutdown system is replaced with a beam regulating system that controls the intensity of the external neutron source. The magnitude of the external neutron source is adjusted by changing the proton beam intensity. It is relevant to consider system disturbances in which the source strength suddenly changes. This could for example happen due to a control system failure, accelerator malfunction, or operator error. The first transient is initiated by ramping the source intensity to double strength while keeping the spatial and energy distribution fixed. The ramp is initiated at t=1 second and halted at 1.001 seconds. The source is held constant thereafter. The reactor is initially at full power; so the disturbance causes a strong overpower condition. In a second transient, the external source neutrons are completely removed, i.e., a source trip.

Fig 2 and Fig 3, display the results for the source overpowers and the source trip events, respectively. The power responds with a prompt jump followed by a slower adjustment when the delayed neutrons establish a balance with the new flux level. In the source removal transient, the power is reduced to a level determined by fissions induced by delayed neutrons plus the release of decay heat. The fission power dies away faster in cores with larger subcriticality because the multiplication of delayed neutrons is lower. The decay power is given by the fission product inventory and its change requires longer time intervals. The effective delayed neutron fraction is 0.186%. The delayed neutrons typically have a small effect in subcritical reactors[20]. Note that case 3 (k_{eff}=0.9987) is very close to criticality (less than β). Consequently the delayed neutrons are much more influential in that case.

It is seen that the point kinetics method, employing no flux shape recalculations, yields extremely accurate solutions for both the source overpower transient and the source trip transient and at all k_{eff}-levels. In fact, the results are indistinguishable as illustrated in Fig 2 and Fig 3. Numerical performance results are presented in 0TABLE IV and TABLE V. The maximal deviations are 0.2% and 0.9% for the source overpowers and source trip transients, respectively. Maximum deviation occurs shortly after the source has been fully inserted/removed, followed by better agreement from that point and forward. Deviation from the point kinetics solution is an indication of flux shape changes. The good agreement suggests that spatial effects are less important. Since the only source for spatial distortion is due to reactivity feedbacks, the good agreement implies that these are small and/or distributed such that no noticeable flux deformation develops. The effect of neglecting the system feedbacks is shown in Fig 4. Evidently, the current ADS features inherent positive reactivity feedbacks. This is attributed to a positive coolant density feedback component, characteristic of a minor-actinide loaded reactor operating on a fast neutron spectrum, whereas the Doppler effect is negligible. As a comparison, it is seen that the error of the point kinetics method is much smaller than the error due to the neglect of thermal feedbacks, *even* in the deeply subcritical case 2 (k_{eff}=0.9798). In the near-critical reactor, this is not so surprising since the feedbacks have a much stronger effect.

The flux shape that develops following a change in the source strength in a subcritical system without feedback is identical to the initial steady-state distribution (except in the case of complete source removal). The adjustment will occur almost instantaneously (within a few tens of prompt periods). A prompt adjustment of the flux shape prevails since the delayed neutrons are less influential; in a critical reactor the delayed neutrons tend to retard the shape transition. Since an external source perturbation, by itself (feedbacks excluded), does not affect the reactivity[21] the point kinetics results typically become quite accurate. In case strong feedbacks occur, the point kinetics approach may not necessarily provide correct results.

In the source trip transient the feedbacks cause the reactivity to decrease. As shown in TABLE V, the point kinetics method has a tendency to overpredict the negative reactivity insertion in the source trip transient. It also appears as if the numerical performance of the point method is improving slightly as the subcriticality decreases. However, it is difficult to draw any firm conclusions on that behavior; all results are very close together. It could be related to the nature and the interplay of the feedbacks in this particular problem. The source overpower transient does not seem to exhibit the same behavior.

Test calculations confirmed that a time step of 10 ms was adequate suggested by the fact that employing time increments of 1 ms and 0.1 ms provided essentially identical results (not shown).

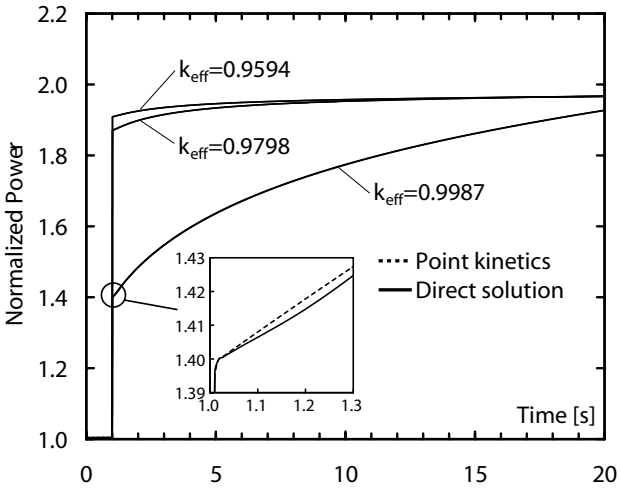

Fig 2. Source overpower transient problem.

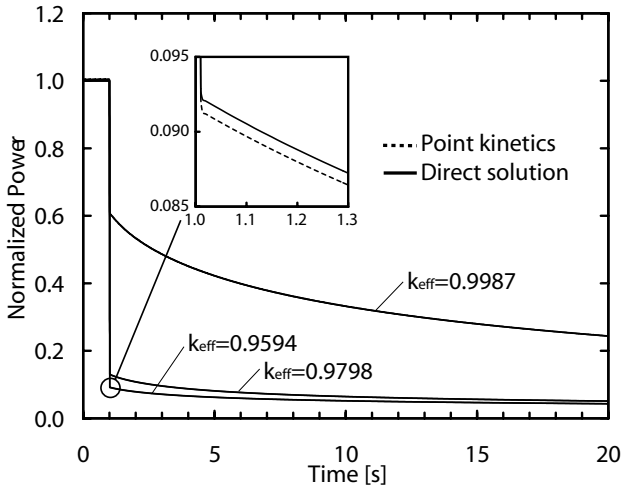

Fig 3. Source trip transient problem.

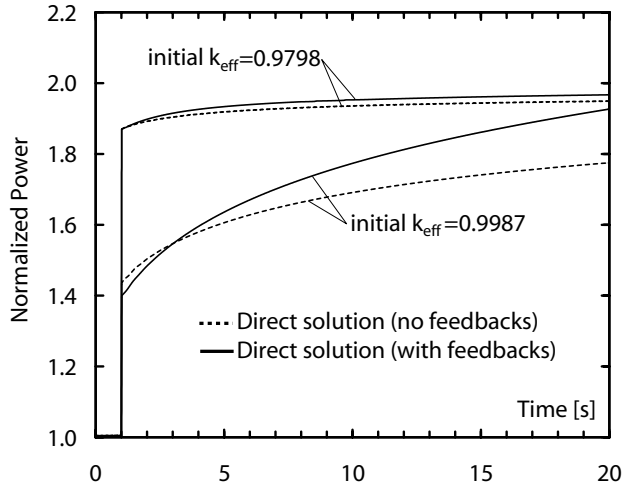

Fig 4. Source overpower transient with and without reactivity feedbacks.

TABLE IV
Comparison of results for the source overpower transient problem[e]

Time	Initial k_{eff}=0.9594			Initial k_{eff}=0.9798			Initial k_{eff}=0.9987		
[s]	Direct	PK	ε (%)	Direct	PK	ε (%)	Direct	PK	ε (%)
2.0	1.9245	1.9251	0.03	1.8981	1.8988	0.04	1.4837	1.4853	0.10
5.0	1.9454	1.9458	0.02	1.9336	1.9339	0.01	1.6357	1.6372	0.10
10.0	1.9570	1.9572	0.01	1.9528	1.9530	0.01	1.7734	1.7746	0.06
15.0	1.9626	1.9626	0.00	1.9613	1.9617	0.02	1.8612	1.8620	0.05
20.0	1.9663	1.9662	0.00	1.9671	1.9673	0.01	1.9268	1.9274	0.03
Max deviation (%)			0.05			0.08			0.22

[e]Direct numerical solution (Direct), point kinetics solution (PK), ε (%) is relative error in calculated power: $(P_{PK}-P_{direct})/P_{direct}$, max deviation is maximum relative error over a 20 sec. time period.

TABLE V
Comparison of results for the source trip transient problem.

Time	Initial k_{eff}=0.9594			Initial k_{eff}=0.9798			Initial k_{eff}=0.9987		
[s]	Direct	PK	ε (%)	Direct	PK	ε (%)	Direct	PK	ε (%)
2.0	0.0791	0.0784	-0.84	0.1084	0.1077	-0.64	0.5342	0.5337	-0.09
5.0	0.0626	0.0622	-0.68	0.0816	0.0811	-0.60	0.4228	0.4223	-0.11
10.0	0.0521	0.0518	-0.54	0.0647	0.0644	-0.50	0.3323	0.3319	-0.09
15.0	0.0468	0.0466	-0.45	0.0565	0.0562	-0.43	0.2797	0.2797	-0.01
20.0	0.0433	0.0432	-0.40	0.0512	0.0510	-0.39	0.2439	0.2436	-0.11
Max deviation (%)			-0.94			-0.73			-0.36

V.B. Localized Reactivity Insertion

In this section, we consider the effect of local reactivity insertions. It is assumed that a fuel subassembly is fully withdrawn at initial conditions and subsequently drops into the core during operation. Despite the hypothetical nature of this scenario, it is useful for evaluating the performance of the underlying kinetics methods. An idealized model of the subassembly movement is employed, in which the volume fraction of materials representing the control subassembly increases uniformly over its axial distance with time. It is further assumed that the subassembly is inserted in a ramp fashion over a time interval of 1 second. The transient is initiated during operation at full power (the external source strength is initially adjusted so that the steady-state reactor power corresponds to the nominal power).

We investigate the effect of reactivity insertion at two different positions; in one instant we move a subassembly close to core-center (subassembly no. 4 in accordance with Fig 1) and in a second study it is inserted close to the core boundary (subassembly no. 16 in accordance with Fig 1). It is assumed that the region representing the absent subassembly is occupied with coolant at initial conditions. In TABLE VI, the initial k_{eff}-values of the various configurations are shown. The Δk_{eff} given in TABLE VI corresponds to the increase in effective multiplication constant when the subassembly is completely inserted, when thermal feedback effects are not included, i.e. it is the numerical difference in the initial k_{eff} when the core is fully loaded (values tabulated in TABLE III) and for the case when one subassembly is absent from start. It is seen that the reactivity worth of the fuel subassembly near the core-center is approximately 13$ and 4$ for the subassembly at the core boundary. It should be noted, however, that starting from normal power and temperature the coolant expansion reactivity coefficient will contribute with some additional reactivity insertion.

TABLE VI

Calculations of the core configurations aimed at studying subassembly movement. Δk_{eff} is the corresponding change in k_{eff} when the subassembly is inserted into the core. The value given in parenthesis is the reactivity insertion quoted in dollars (1$=0.00186).

Core configuration	Insertion close to core-center		Insertion close to core boundary	
	Intial k_{eff}	Δk_{eff} [f]	Intial k_{eff}	Δk_{eff} [f]
Case 1	0.9356	+0.0238 (+12.8)	0.9519	+0.0075 (+4.0)
Case 2	0.9558	+0.0240 (+12.9)	0.9722	+0.0076 (+4.1)
Case 3	0.9746	+0.0241 (+13.0)	0.9910	+0.0077 (+4.1)

[f]Change in k_{eff} when feedbacks are not taken into account. The amount of reactivity inserted in cases 2 and 3 is slightly higher because of a higher reactivity worth of individual fuel subassemblies.

It is well known, from critical system analysis that for local reactivity insertion events, using the point kinetics technique to calculate the response can lead to significant errors. This is because the basic assumption is that the flux shape remains constant. Comparison with the exact results shows that this is indeed the case. The point approximation severely underestimates the excursion for the case that is closest to the critical state (initial k_{eff}=0.9746), shown in Fig 5. However, it is seen that point kinetics is a much better approximation for the deeply subcritical cores, illustrated in Fig 6. In TABLE VII, the relative root-mean-square (*RelRMS*) deviation of the local peak-to-average flux (for all three-dimensional spatial nodes) with respect to the initial distribution is shown. Comparing the *RelRMS* values for the various subcritical test cases provide an indication of the flux spatial distortion sensitivity as function reactor k_{eff}. While the amount of reactivity insertion is essentially the same for all test configurations, the *RelRMS* variation of the flux shape decreases, as the core multiplication constant decreases. Thus, it appears that for a fixed reactivity change the flux spatial distortion decreases when the system is more subcritical. This behavior seems reasonable considering the reduced sensitivity to reactivity inputs in the subcritical state. As the subcritical margin increases, the total (negative) reactivity of the system increases and a given reactivity change will constitute a smaller fraction of the overall reactivity. The net effect is lower reactivity sensitivity as the subcriticality increases. When the fuel subassembly falls into the reactor, the neutron flux increases near this location due to a local increase in the fission rate. In the near-critical reactor, the neutrons are strongly multiplied, and the increase in the fission source produces a local deformation of the flux shape. In a deeply subcritical core, the neutrons are weakly multiplied therefore; the insertion of the subassembly has an overall smaller effect. Due to this lower sensitivity, flux distortions following a reactivity disturbance diminish as the k_{eff} decreases.

In the second problem, the subassembly is inserted at the outer end of the core (subassembly no. 16 according to Fig. 1). Given the lower importance in the outer core regions, the magnitude of the reactivity disturbance is lower. The spatial location of the initiating perturbation is expected to influence the resulting flux deformation. The point method showed a slight improvement, however, the basic trends were the same, producing better results at lower subcriticality levels. The *RelRMS* deviation in the flux spatial distribution is summarized in TABLE VIII.

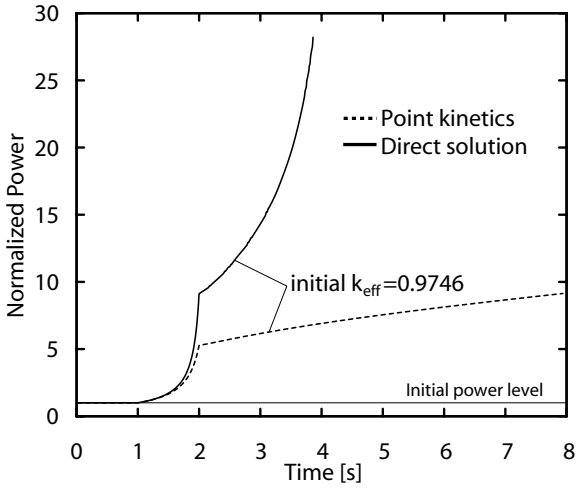

Fig 5. Reactivity insertion near core-center (initial k_{eff}=0.9746).

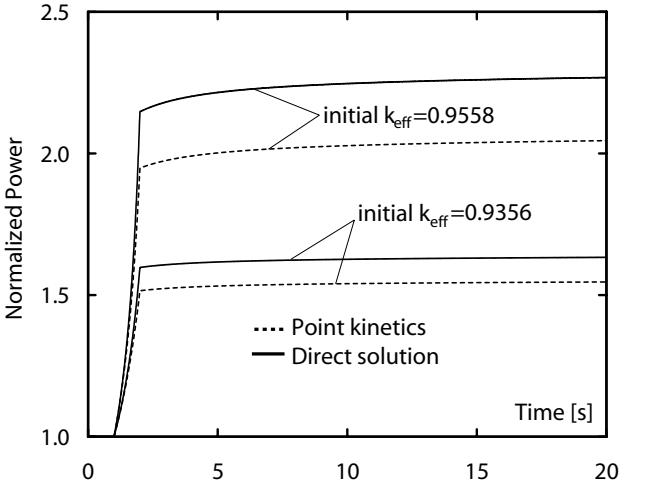

Fig 6. Reactivity insertion near core-center (initial k_{eff}=0.9356 and k_{eff}=0.9558).

TABLE VII

Relative root-mean-square (*RelRMS*) difference of the peak-to-average flux distribution with respect to the initial flux distribution following insertion of the subassembly near the core-center.

Time [s]	RelRMS[g] peak-to-average flux		
	Initial k_{eff}=0.9356	Initial k_{eff}=0.9558	Initial k_{eff}=0.9746
1.2	0.9%	1.0%	1.2%
1.4	1.8%	2.2%	2.6%
1.6	2.8%	3.4%	4.1%
1.8	4.0%	4.7%	5.7%
2.0	5.2%	6.2%	7.4%
3.0	5.2%	6.3%	7.8%
20.0	5.4%	6.6%	-

[g] $RelRMS = \sqrt{\frac{1}{N}\sum_{i=1}^{N}\left(\frac{p_i - p_{0_i}}{p_{0_i}}\right)^2}$ where N is the number of hex-Z nodes in the three-dimensional space and p is the local peak-to-average flux in each node. The subscript 0 denotes the initial state.

TABLE VIII

Relative root-mean-square (*RelRMS*) difference of the peak-to-average flux distribution with respect to the initial flux distribution following insertion of the subassembly near the core boundary.

Time [s]	RelRMS peak-to-average flux		
	Initial k_{eff}=0.9519	Initial k_{eff}=0.9722	Initial k_{eff}=0.9910
1.2	0.7%	0.8%	0.9%
1.4	1.4%	1.6%	1.8%
1.6	2.2%	2.6%	2.9%
1.8	3.0%	3.6%	4.0%
2.0	4.0%	4.7%	5.3%
3.0	4.0%	4.7%	5.5%
20.0	4.1%	4.8%	-

Numerical performance data are summarized in TABLE IX for the case when the subassembly is inserted close to core-center and in TABLE X for the case when the subassembly is inserted at the core boundary. Ideally (stripped of reactivity feedbacks), all cases should remain in the subcritical state even after the subassembly has been fully inserted. However, due to positive thermal feedbacks additional reactivity is inserted, which for the case with initial k_{eff}=0.9746 (subassembly inserted close to core-center) leads to an excursion in the range above critical (but below prompt critical). The direct space-time solution predicts that the reactor in that case becomes supercritical at t=3.3 seconds and the calculation is subsequently terminated at t=3.9 seconds due to reaching excessive temperatures. The point solution, on the other hand, underpredicts the reactivity insertion and the reactor remains in the subcritical range, which leads to considerable discrepancies since it is in the supercritical range where most of the power rise occurs. The cases k_{eff}=0.9356 and k_{eff}=0.9558 are predicted to stay in the subcritical state, therefore the power approaches a stationary level and the error is essentially bounded at the value already accumulated. It is seen that the point kinetics calculations underestimate the exact space-time solution in all cases. The same non-conservative behavior is observed in critical systems.

The fuel is calculated to reach the melting point at approximately 2.6 sec. into the transient. In reality, the nature of the accident might change significantly from that point. Fuel dispersal may act to terminate the accident prior to reaching supercritical conditions, however, reactivity could also be added due to fuel relocation and expulsion of lead-bismuth. Therefore, current predictions beyond core damaging levels are highly uncertain from a physical point of view, but nonetheless it permits comparison of the basic methods under extreme conditions.

TABLE IX

Comparison of results for the insertion of a fuel subassembly near the core-center (subassembly no. 9 according to the core map in Fig. 1).

Time	Initial k_{eff}=0.9356			Initial k_{eff}=0.9558			Initial k_{eff}=0.9746		
[s]	Direct	PK	ε (%)	Direct	PK	ε (%)	Direct	PK	ε (%)
1.2	1.073	1.072	-0.1	1.108	1.106	-0.2	1.191	1.187	-0.3
1.4	1.163	1.156	-0.6	1.250	1.238	-0.9	1.493	1.464	-1.9
1.6	1.274	1.255	-1.5	1.442	1.408	-2.4	2.034	1.920	-5.6
1.8	1.415	1.372	-3.0	1.719	1.633	-5.0	3.282	2.807	-14.5
2.0	1.598	1.515	-5.2	2.148	1.948	-9.3	9.112	5.270	-42.2
3.0	1.607	1.523	-5.2	2.182	1.975	-9.5	14.314	6.157	-57.0
20.0	1.633	1.546	-5.3	2.268	2.045	-9.8	-	-	-
Max deviation (%)			-5.3			-9.8			-75.9

TABLE X

Comparison of results for the insertion of a fuel subassembly near the core-boundary (subassembly no. 16 according to the core map in Fig. 1).

Time	Initial k_{eff}=0.9519			Initial k_{eff}=0.9722			Initial k_{eff}=0.9910		
[s]	Direct	PK	ε (%)	Direct	PK	ε (%)	Direct	PK	ε (%)
2.0	1.136	1.106	-2.63	1.290	1.223	-5.18	3.382	2.380	-29.6
4.0	1.138	1.108	-2.66	1.302	1.232	-5.44	4.687	2.734	-41.7
6.0	1.140	1.109	-2.71	1.307	1.235	-5.50	6.058	2.941	-51.5
8.0	1.141	1.110	-2.72	1.311	1.237	-5.58	7.980	3.082	-61.4
10.0	1.141	1.110	-2.72	1.312	1.239	-5.56	12.815	3.188	-75.1
20.0	1.143	1.111	-2.75	1.317	1.243	-5.65	-	-	-
Max deviation (%)			-2.77			-5.65			-78.2

V.C. Flow Reduction

Finally, kinetics performance characteristics were compared for a flow coastdown event. Complete loss of forced flow in the primary system is assumed. The analysis further assumes that the shutdown system is inoperable, which in an accelerator-driven system corresponds to a "beam-on" situation. Constant coolant inlet temperature is specified.

The power traces for the cases with initial k_{eff}=0.9594 and k_{eff}=0.9798 are presented in Fig 7 and for k_{eff}=0.9987 in Fig 8; the scale on the left is for the normalized power, and the scale on the right is for the normalized flow. The accident is initiated by gradually reducing the inlet driving

pressure, starting at t=1 sec. The pump driving pressure approaches zero at 10 sec. The transient is dictated by coolant reactivity feedback. Coolant heat-up occurs at a rate determined by the flow coastdown. The resulting density reduction of the coolant has a positive effect. For the deeply subcritical cores, i.e, cases k_{eff}=0.9594 and k_{eff}=0.9798, the power peaks (with some delay) as the flow drops to a minimum. Eventually, the coolant flow balances at a flowrate sustained by natural circulation alone. Given the small reactivity effects, the power settles at a level slightly above the initial state. For the near-critical core, shown in Fig 8, the power trace is different. The feedback-induced reactivity has a much stronger effect in this case. This is because the response is more sensitive near the critical state. At approximately 13.8 seconds into the transient, the reactor becomes supercritical. Continued coolant heat-up causes gradual insertions of reactivity, leading to an essentially unbounded power excursion. The calculation was terminated when the cladding in the hottest channel exceeded the melting point.

In TABLE XI, the numerical error versus time is presented. The point kinetics results were found to be in excellent agreement with the exact solution for the deeply subcritical cases (initial k_{eff}=0.9594 and k_{eff}=0.9798), indicating that coolant feedbacks did not alter the initial flux shape. For the near-critical reactor (initial k_{eff}=0.9987), the direct solution predicts a somewhat higher power than does the point approximation.

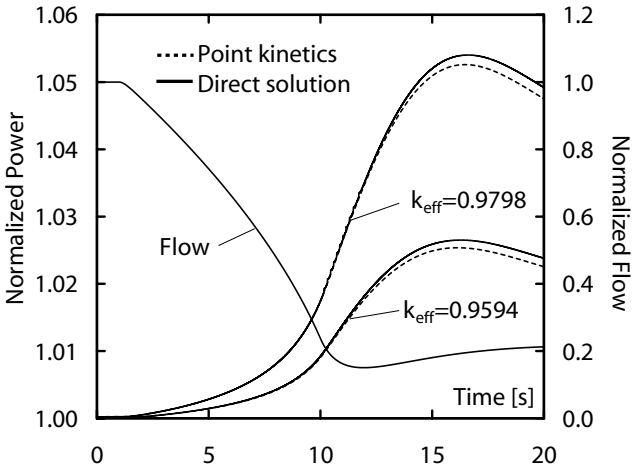

Fig 7. Unprotected Loss-of-flow transient (initial k_{eff}=0.9594 and k_{eff}=0.9798).

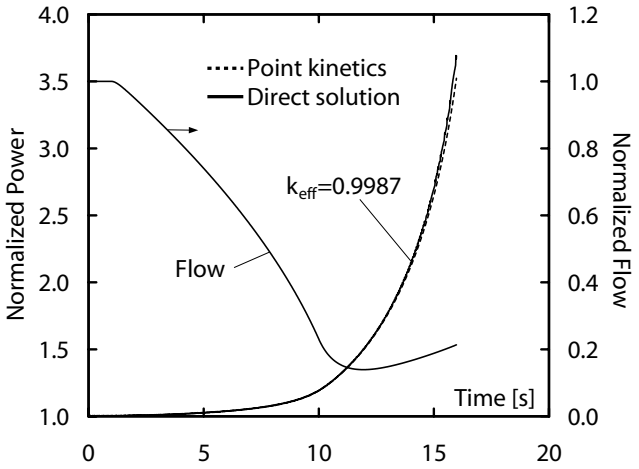

Fig 8. Unprotected Loss-of-flow transient (initial k_{eff}=0.9987).

TABLE IX
Comparison of results for the Unprotected Loss-of-Flow transient.

Time	Initial k_{eff}=0.9594			Initial k_{eff}=0.9798			Initial k_{eff}=0.9987		
[s]	Direct	PK	ε (%)	Direct	PK	ε (%)	Direct	PK	ε (%)
2.0	1.0002	1.0002	0.00	1.0004	1.0005	0.01	1.0036	1.0058	0.22
5.0	1.0014	1.0014	0.01	1.0030	1.0028	-0.01	1.0244	1.0267	0.23
10.0	1.0093	1.0090	-0.03	1.0176	1.0175	-0.02	1.1908	1.1915	0.06
15.0	1.0259	1.0249	-0.10	1.0521	1.0509	-0.11	2.6999	2.6493	-1.87
20.0	1.0238	1.0225	-0.12	1.0492	1.0475	-0.16	-	-	-
Max deviation (%)			-0.14			-0.19			-4.56

VI. CONCLUSIONS

The purpose of this paper was to investigate the ability of point kinetics to predict the transient behavior in accelerator-driven systems (ADS) under accident conditions. Numerical experiments were carried out in a minor-actinide loaded and lead-bismuth cooled ADS. The precision of the point approximation was compared in the subcritical range from k_{eff}=0.9594 to 0.9987. A full three-dimensional nodal energy-space-time solution, coupled with feedback effects, was provided and used as a standard of comparison. The numerical tests suggest that point kinetics is capable of producing very good predictions of certain types of accidents in ADS's. For transients involving external source perturbations the point method provided extremely accurate results. Such changes are associated with spatially uniform reactivity feedbacks that produce little flux deformation. This may not be the case in severe source disturbances, involving strong reactivity feedbacks, but for most practical situations, it is expected that source disturbances be rather well described by point kinetics. When applied to the analysis of localized reactivity perturbations - a condition when the point treatment is expected to be a poor approximation - the results indicated better precision at lower k_{eff}-levels. This behavior appears to be due to the lower reactivity sensitiveness in the subcritical operating state, which effectively weakens the response and mitigates any spatial distortions. If a subcritical reactor is subject to a change in

the strength of the external source, or a change in reactivity within the subcritical range, the neutron population will adjust to a new stationary level. Therefore, within the normal range of operation, the power predicted by the point kinetics method and the associated error in comparison with the exact solution tends to approach an essentially bounded value. This is quite the contrary of critical reactors, in the absence of reactivity feedbacks the response will either diverge exponentially or decay to zero depending on the sign of the reactivity disturbance. In general, the flux shape in a fast neutron spectrum shows strong space-time coupling, i.e., local spatial disturbances are rapidly distributed to the remaining parts of the core, which softens spatial variations in a transient. This is usually attributed to the relatively large mean free path of fast neutrons and to the comparatively compact core size of a fast reactor. Due to the overall smaller influence of delayed neutrons in the subcritical operating state a prompt adjustment of the flux shape prevails. For a critical reactor, the delayed neutrons tend to retard the shape transition for certain transients. All together these characteristics are favorable from a point kinetics view of application to fast spectrum ADS systems. A non-favorable feature is that proposed ADS designs have large reactivity potential vested in the core[22]. Changes in lattice geometry or coolant density[23] may contribute with significant reactivity values. Such feedbacks are potential sources of spatial effects, and therefore, possible deviation from the point kinetics model. The essential requirements for an accurate point kinetics treatment are the same in subcritical reactors, i.e., symmetric reactivity insertion, small and tightly coupled core. Thus, favorable point kinetics performance in an ADS appears to be possible as long as the transient does not involve significant shape distortions. Similar conclusions have been drawn by other authors[24]. While the current study suggests that subcritical operation may provide for improved point kinetics performance and enhanced tolerance to system reactivity perturbations, the results showed that it is not feasible for local reactivity perturbation studies and it should still be used with care in situations involving strong feedback phenomena.

The situation in a loss-of-flow scenario was also studied. Here again, the point method was capable of very accurate calculations. The reasons are similar to those previously discussed. It was also found that the point kinetics model has a tendency to underestimate the severity of reactivity insertion accidents. The same nonconservative behavior is observed in critical systems, but it ought to be recognized for subcritical systems as well because of its overriding importance in reactor safety considerations.

VII. ACKNOWLEDGMENTS

This research was supported by the Swedish Nuclear Fuel and Waste Management Co. (SKB). The calculations reported here were performed on the ANL-NE computer network.

REFERENCES

1. A. RINEISKI and W. MASCHEK, "On Application of Quasistatic and Point-Kinetics Schemes for Subcritical Systems With External Neutron Source," Nuclear Mathematical and Computational Sciences: A Century in Review - A Century Anew, M&C 2003, Gatlinburg, Tennessee, USA, April 6-11 (2003).

2. D. G. CACUCI, "On Perturbation Theory and Reactor Kinetics: From Wigner's Pile Period to Accelerator Driven Systems," PHYSOR 2002, Seoul, Korea, October 7-10 (2002).

3. A. F. HENRY, "The Application of Reactor Kinetics to the Analysis of Experiments," *Nuclear Science and Engineering,* **3**, 52-70 (1958).

4. E. P. GYFTOPOULOS, Chapter on "General Reactor Dynamics," in *The Technology of Nuclear Reactor Safety*, Vol. 1, p. 175-204, T. J. THOMPSON and J. G. BECKERLY, Eds., The MIT Press, Cambridge, Massachusetts, USA (1964).

5. J. B. YASINSKY and A. F. HENRY, "Some Numerical Experiments Concerning Space-Time Reactor Kinetics Behavior," *Nuclear Science and Engineering,* **22**, 171-181 (1965).

6. K. O. OTT and D. A. MENELEY, "Accuracy of the Quasistatic Treatment of Spatial Reactor Kinetics," *Nuclear Science and Engineering*, **36**, 402-411 (1969).

7. A. F. HENRY, *Nuclear-Reactor Analysis,* p. 300-329, The MIT Press, Cambridge, Massachusetts, USA (1975).

8. K. O. OTT and R. J. NEUHOLD, *Introductory Nuclear Reactor Dynamics,* p. 69, American Nuclear Society, LaGrange Park, Illinois, USA (1985).

9. M. BECKER, "A Generalized Formulation of Point Nuclear Reactor Kinetics Equations," *Nuclear Science and Engineering*, **31**, 458-464 (1968).

10. "Comparison Calculations for an Accelerator-driven Minor Actinide Burner," OECD/NEA Nuclear Science Committee, NEA/NSC/DOC(2001)13, OECD (2002). Benchmark prepared by P. WYDLER and H. TAKANO, NEA/NSC/DOC(99)13, Revised 27 Aug. 1999.

11. M. SALVATORES, et al., "Long-lived radioactive waste transmutation and the role of accelerator driven (hybrid) systems," *Nucl. Instrum. Methods Phys. Res., Sect. A*, **414**, 5-20 (1998).

12. J. E. CAHALAN, T. AMA, G. PALMIOTTI, T. A. TAIWO, and W. S. YANG, "Development of a Coupled Dynamics Code with Transport Theory Capability," PHYSOR 2000, Pittsburgh, USA, 7-11 May (2000).

13. H. HENRYSON II, B. J. TOPPEL, and C. G. STENBERG, "MC^2-2: A Code to Calculate Fast Neutron Spectra and Multigroup Cross Sections," ANL-8144, Argonne National Laboratory (1976).

14. R. E. ALCOUFFE, F. W. BRINKLEY, D. R. MARR, and R. D. O'DELL, "User's Guide for TWODANT: A Code Package for Two-Dimensional, Diffusion-Accelerated, Neutral-Particle Transport," LA-10049-M, Los Alamos National Laboratory (1990).

15. R. D. LAWRENCE, "The DIF3D Nodal Neutronics Option for Two- and Three-Dimensional Diffusion Theory Calculations in Hexagonal Geometry," ANL-83-1, Argonne National Laboratory (1983).

16. T. A. TAIWO, "DIF3D-K: A Nodal Kinetics Code for Solving the Time-Dependent Diffusion Equation in Hexagonal-Z Geometry," ANL/NPR-92/17, Argonne National Laboratory (1992).

17. W. M. STACEY, Jr., *Space-Time Nuclear Reactor Kinetics*, p. 43-46, Academic Press, New York, USA (1969).

18. R. D. LAWRENCE, "Perturbation Theory Within the Framework of a Higher-Order Nodal Method," *Trans. Am. Nucl. Soc.,* **46**, 402 (1984).

19. T. A. TAIWO, H. S. KHALIL, J. E. CAHALAN, and E. E. MORRIS, "Time-Step Selection Considerations in the Analysis of Reactor Transients with DIF3D-K," ," *Trans. Am. Nucl. Soc.,* **68**, 429-430 (1993).

20. R. A. RYDIN and M. L. WOOSLEY, JR., "Evidence of Source Dominance in the Dynamic Behavior of Accelerator-Driven Systems," *Nuclear Science and Engineering*, **126**, 341-344 (1997).

21. Y. KIM, W. S. YANG, T. A. TAIWO, and R. N. HILL, "Reactivity Estimation for Source-Driven Systems Using First-Order Perturbation Theory," PHYSOR 2002, Seoul, Korea, October 7-10 (2002).

22. W. MASCHEK, A. RINEISKI, K. MORITA, M. FLAD, "Inherent and Passive Safety Measures in Accelerator Driven Systems: A Safety Strategy for ADS," GLOBAL 2001, Paris, France, Sep 9-13 (2001).

23. M. ERIKSSON, J. WALLENIUS, J. E. CAHALAN, K. TUCEK, and W. GUDOWSKI, "Safety analysis of Na and Pb-Bi coolants in response to beam instabilities," Proc. 3rd International Workshop on Utilisation and Reliability of High Power Proton Accelerators, Santa Fe, USA, May (2002).

24. A. AMIONE, et al., "Dynamics of Accelerator-Driven Systems by the Quasi-static Method," 6th International Meeting on Nuclear Applications of Accelerator Technology (AccApp'03), June 1-5, San Diego (2003).